Multi-shell Nanostructures Minimize Diffusion Pathways and Dual Active Sites Decouple Activation for Efficient Ammonia Borane Hydrolysis

Lei Liu#, Zijian Zhou#, Ying Liu, Xin Yu*, Dunxi Yu*, Minghou Xu

State Key Laboratory of Coal Combustion, School of Power and Engineering, Huazhong University of Science and Technology, Wuhan 430074, China

*Corresponding Author: xinyu@hust.edu.cn (Xin Yu); yudunxi@hust.edu.cn (Dunxi Yu)

#These authors contributed equally.

This SM includes:

- **Computational Details;**
- **Table S1 Specific surface area and pore volume of each catalyst;**
- **Fig. S1 Mean Squared Displacement (MSD) of H_2O on Co_3O_4 slab;**
- **Fig. S2 Mean Squared Displacement (MSD) of NH_3BH_3 (AB) on Co_3O_4 slab;**
- **Fig. S3. The crystal slabs of M_3O_4 (M=Co, Zn, Ga, Cu, Ni, Fe and Mn) for H2O and NH_3BH_3 (AB);**
- **Fig. S4 Mass change of catalyst precursors during the calcination process;**
- **Fig. S5. High-magnification SEM images of (a) CoCu-HS and (b) CoCu-SG. The statistical analysis of the particle size distribution for (c) CoCu-HS and (d) CoCu-SG.**
- **Fig. S6 SEM-EDS and HR-TEM of catalyst: Spherical morphology. (a) CoCu-HS, (b) CoNi-HS and (c) CoMn-HS. Lattice fringes (d) CoNi-HS, (e) CoZn-HS and (f) CoMn-HS.**
- **Fig. S7. Various shell thickness CoCu catalysts. (a-c) 0.48±0.32 μm, (d-f) 1.07±0.26 μm and (g-i) 1.62±0.21 μm.**
- **Fig. S8. Catalytic hydrolysis performance for various shell thickness CoCu catalysts: (a) H2 production curve and (b) TOF value of hydrolyzed AB in 0.5mol/L NaOH at 25°C under the action of various catalysts;**
- **Fig. S9. H_2 production curve CoCu-HS with 2 mmol of AB dissolved in 1 mol/L NaOH aqueous solution (5 mL).**
- **Fig. S10 Pore structure for MCo-HS (M=Cu, Ni, Zn and Mn);**
- **Fig. S11 Pore structure for CuCo-HS and CuCo-SG;**
- **Fig. S12 XPS of (a) Co 2p spectrum and (b) Cu 2p spectrum.**
- **Fig. S13 Top view and side view of H_2O and AB adsorption on Co_3O_4 and CuCo-HS.**
- **Fig. S14 Influence of different proportions of Cu on Co_3O_4 catalyst: (a) Phase compositions and (b) TOF values.**

Computational Details

Density Functional Theory (DFT) Structural Optimization: The calculations were performed using with the DS-PAW method (HZWTECH, Shanghai, China). Pseudopotentials were utilized to describe the core electrons, and plane-wave basis sets with a kinetic energy cutoff of 400 eV were adopted to treat the valence electrons. Dispersion corrections were included using the Grimme-D3 method. The Brillouin zone was sampled using a Monkhorst-Pack grid with a (4×4×1) mesh. Convergence criteria were set to ensure that the energy difference per atom was below 1.0×10^{-4} eV and the residual force on all atoms was less than 0.05 eV/Å. The slabs were built with vacuum layer thicknesses larger than 15 Å to avoid the interaction between two periodic slabs. The adsorption energy was calculated by Eq. (Sa).

$$E_{adsorption} = E_{adsorbate+reactant} - E_{Reactant} - E_{adsorbate} \quad \text{(S1)},$$

where, $E_{adsorbate+reactant}$ is the gross system energy of the adsorbates adsorbed on the surface, eV; $E_{Reactant}$ and $E_{adsorbate}$ represent energies of the surface and adsorbate, respectively, eV. In this study, The Gibbs free energy for analysis were used (by considering the entropic change and zero-point energy). The Gibbs free energies were calculated as follows:

$$G = E_e + E_{ZPE} + \Delta TS \quad \text{(S2)},$$

where G represents the Gibbs free energy, E_e represents the DFT calculated energy, E_{ZPE} represents the zero-point energy, and ΔTS represents the entropic change.

Ab Initio Molecular Dynamics (AIMD): The AIMD simulation module embedded in the DS-PAW (HZWTECH, Shanghai, China) was employed, utilizing a time step of 1 fs and the NVT ensemble with the Nose-Hoover thermostat. Geometries were deemed relaxed when the forces on each atom fell below 0.05 eV/Å. Following AIMD simulations, the postprocessing program was used to obtain the mean square displacement (MSD) of the atoms. According to Fick's diffusion law:

$$J = D\frac{\Delta\mu}{\Delta r} \quad \text{(S3)},$$

where J is the diffusion flux of the reactant (H_2O, NH_3BH_3), D is the diffusion coefficient, Δu is the chemical potential, and Δr is the radial gradient of diffusion. The diffusion distance X and time t are related by:

$$X = \sqrt{Dt} \quad \text{(S4)},$$

The diffusion coefficient D was calculated from the mean square displacement (MSD) of H_2O and NH_3BH_3 using:

$$D = \lim_{t\to\infty}\left(\frac{1}{2dt}\langle\vec{r}(t)\rangle\right) \quad \text{(S6)},$$

Here, d is the dimension (d=3), $r(t)^2$ is MSD, and t is the simulation time. Previous studies have shown that the activation energy E_a can be derived from the diffusivity-temperature plot:

$$D = D_0 e^{-\frac{\Delta H}{RT}} \quad \text{(S7)},$$

Table S1 Specific surface area and pore volume of each catalyst

Catalysts	BET surface area (m^2/g)	Pore volume (m^3/g)
CuCo-SG	5.82	0.033
CuCo-HS	98.26	0.211
NiCo-HS	72.38	0.119
ZnCo-HS	55.79	0.116
MnCo-HS	26.88	0.098
Co-HS	25.00	0.095

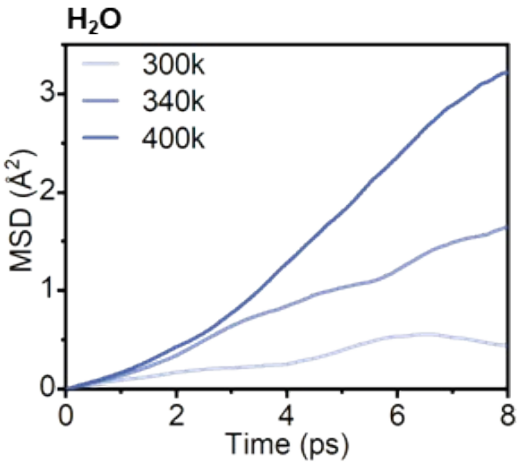

Fig. S1 Mean Squared Displacement (MSD) of H_2O on Co_3O_4 slab.

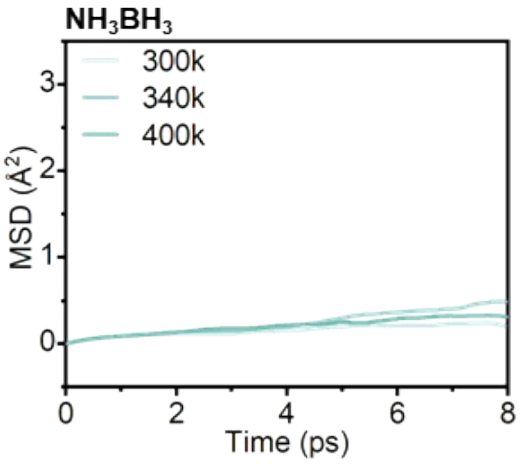

Fig. S2 Mean Squared Displacement (MSD) of NH_3BH_3 (AB) on Co_3O_4 slab.

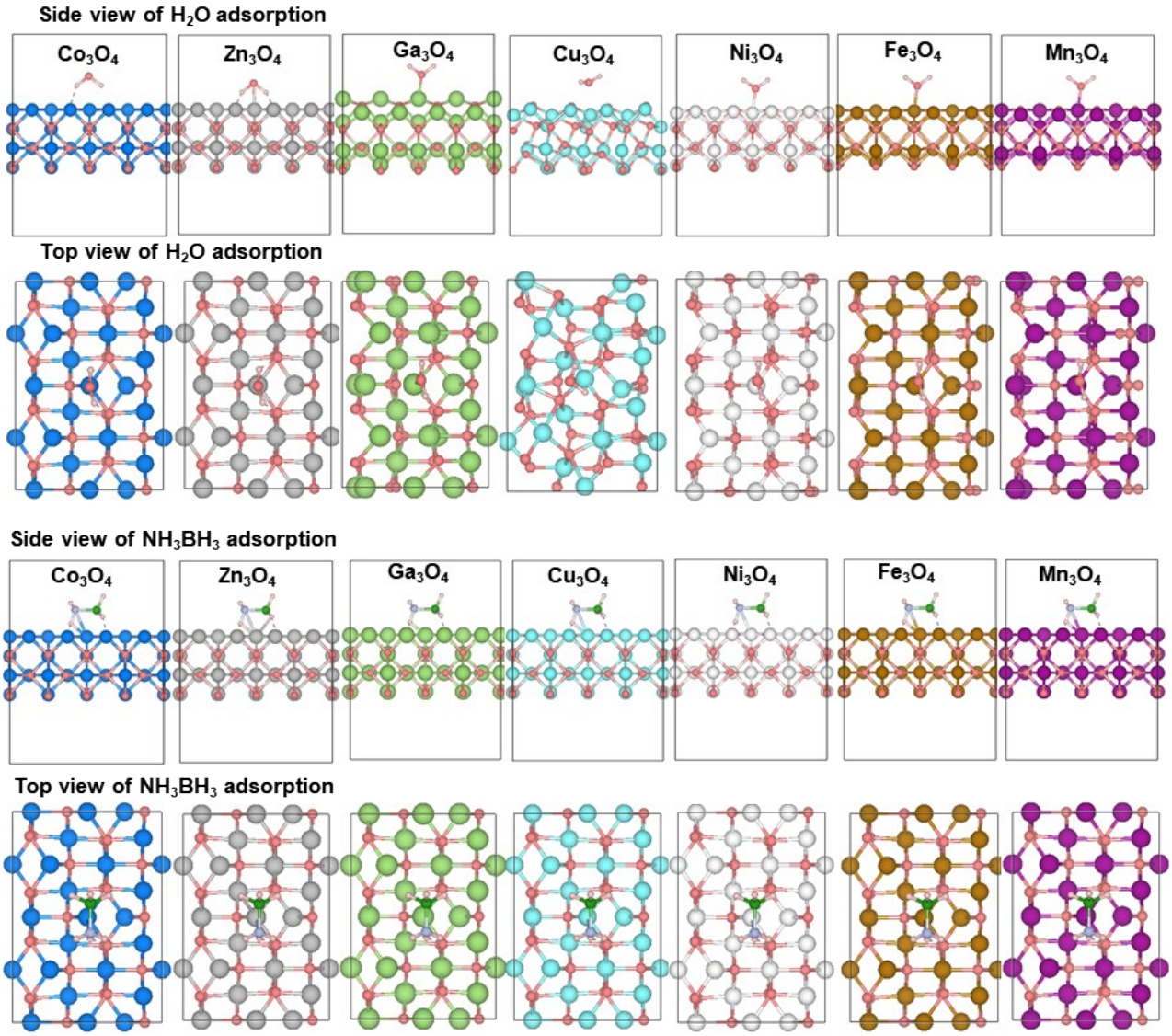

Fig. S3. The crystal slabs of M_3O_4 (M=Co, Zn, Ga, Cu, Ni, Fe and Mn) for H_2O and NH_3BH_3 (AB).

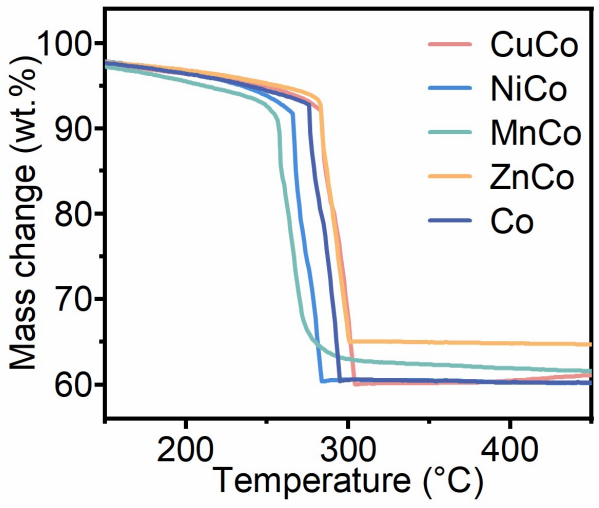

Fig. S4 Mass change of catalyst precursors during the calcination process.

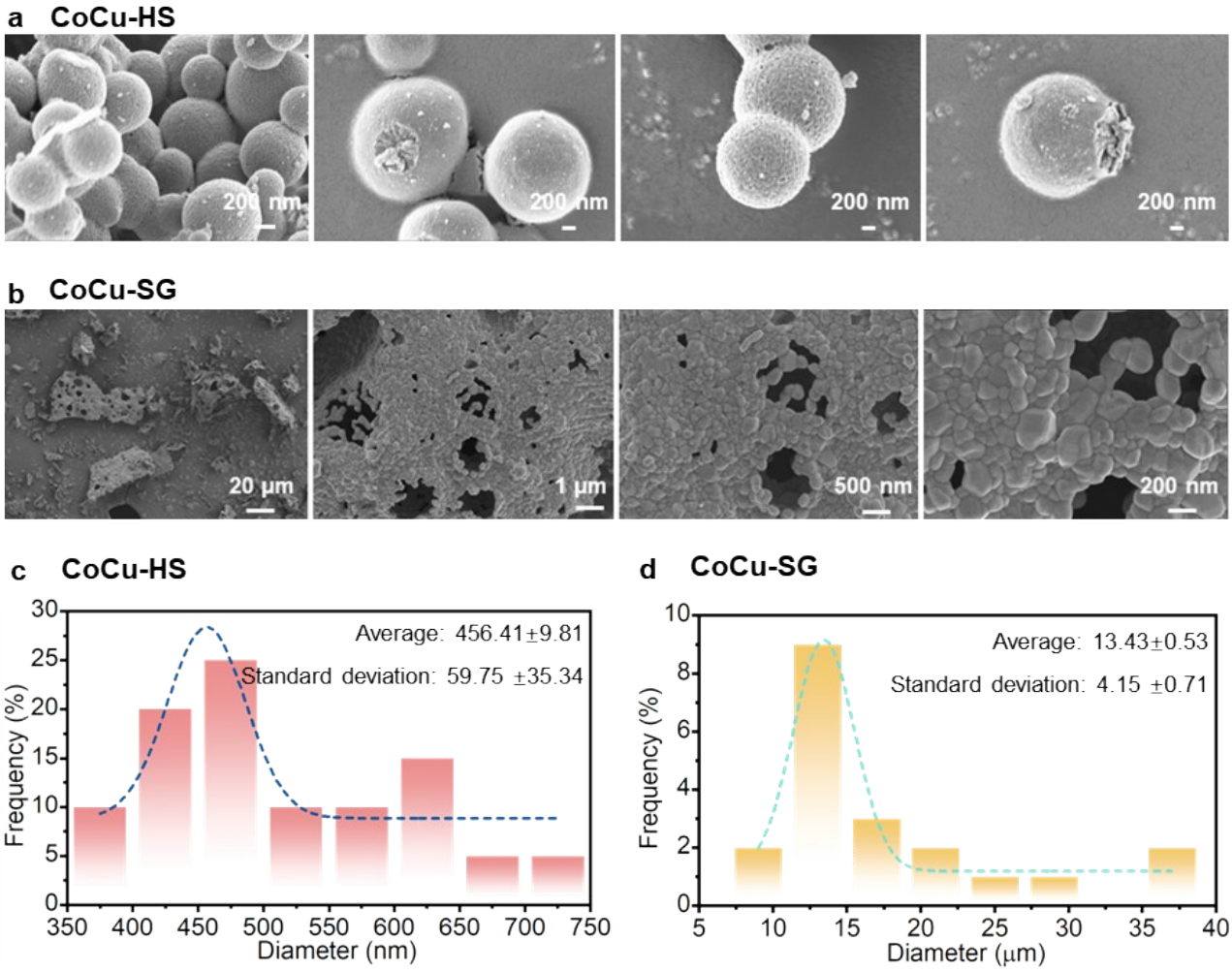

Fig. S5. High-magnification SEM images of (a) CoCu-HS and (b) CoCu-SG. The statistical analysis of the particle size distribution for (c) CoCu-HS and (d) CoCu-SG.

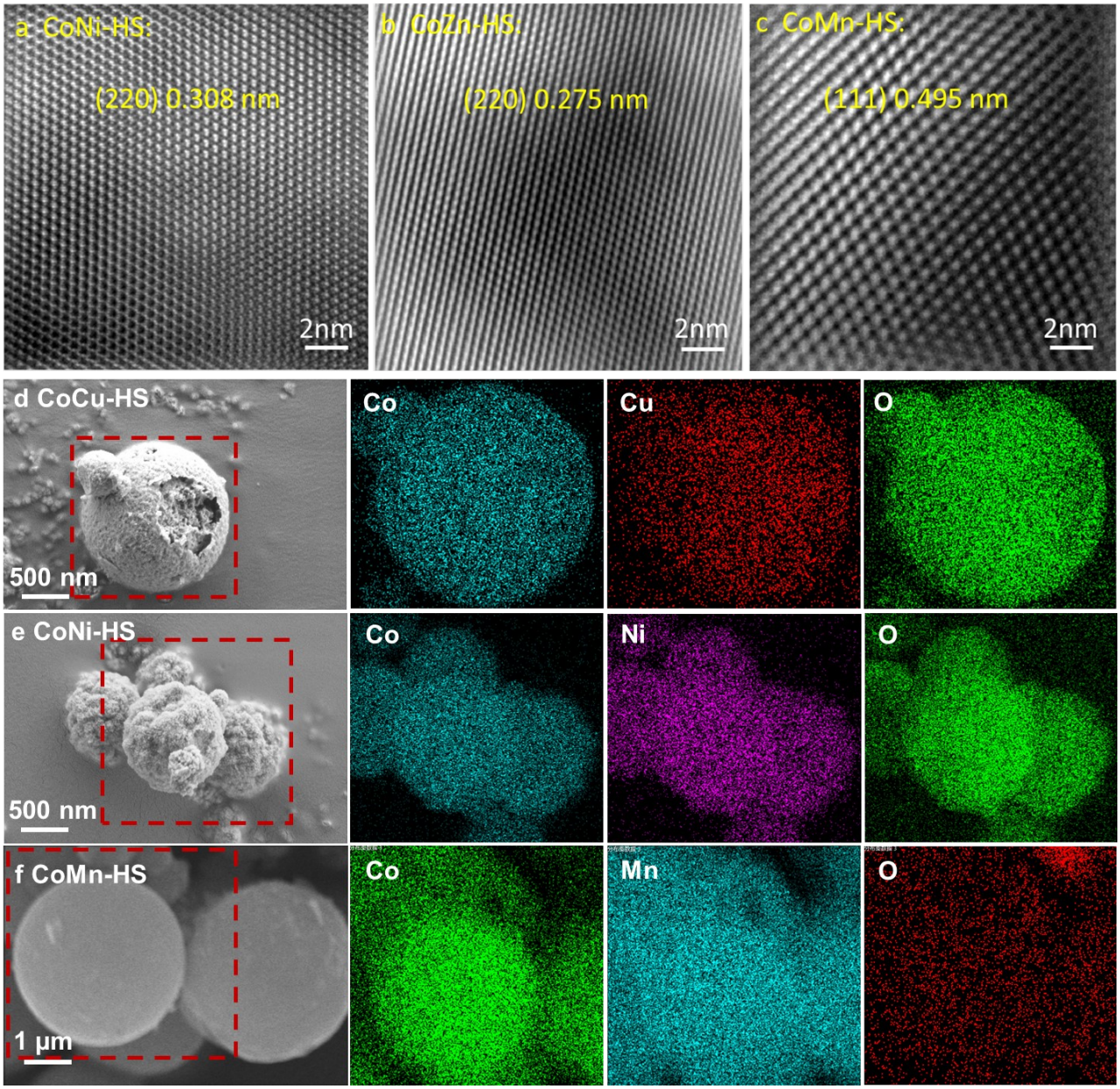

Fig. S6 SEM-EDS and HR-TEM of catalyst: Spherical morphology. (a) CoCu-HS, (b) CoNi-HS and (c) CoMn-HS. Lattice fringes (d) CoNi-HS, (e) CoZn-HS and (f) CoMn-HS.

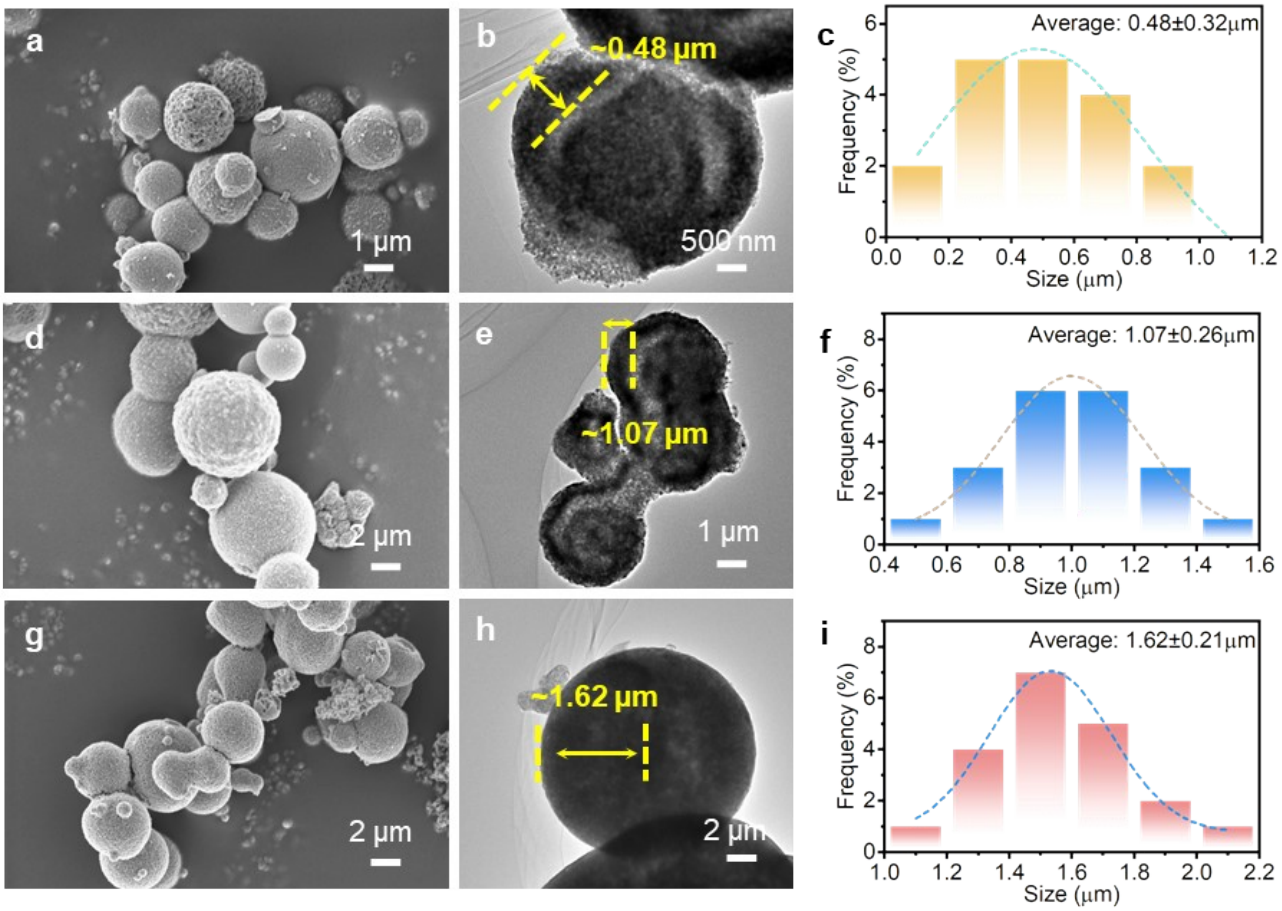

Fig. S7. Various shell thickness CoCu catalysts. (a-c) 0.48±0.32 μm, (d-f) 1.07±0.26 μm and (g-i) 1.62±0.21 μm.

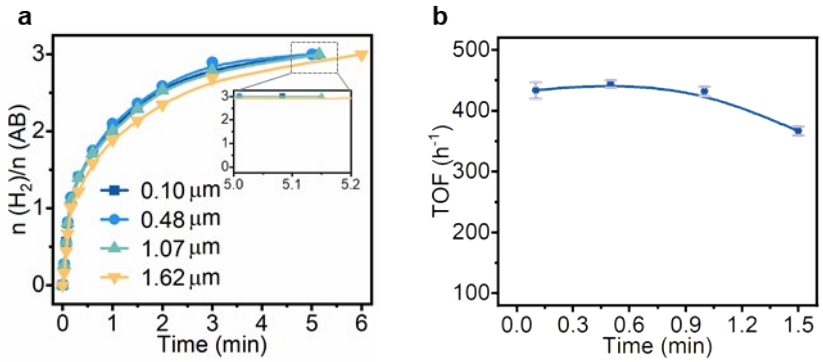

Fig. S8. Catalytic hydrolysis performance for various shell thickness CoCu catalysts: (a) H_2 production curve and (b) TOF value of hydrolyzed AB in 0.5mol/L NaOH at 25°C under the action of various catalysts;

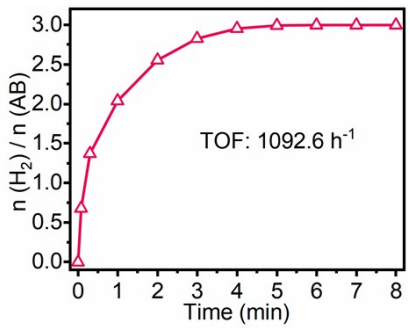

Fig. S9. H_2 production curve CoCu-HS with 2 mmol of AB dissolved in 1 mol/L NaOH aqueous solution (5 mL).

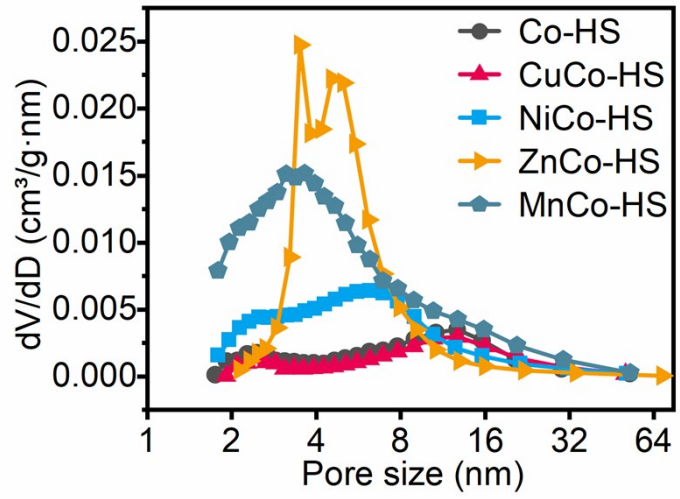

Fig. S10 Pore structure for MCo-HS (M=Cu, Ni, Zn and Mn).

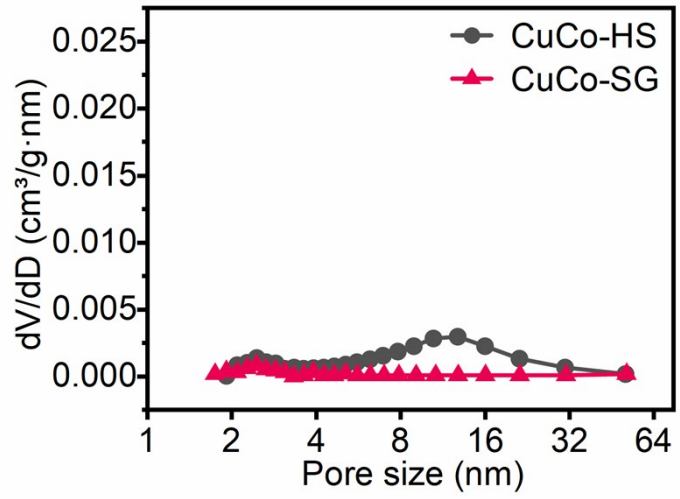

Fig. S11 Pore structure for CuCo-HS and CuCo-SG.

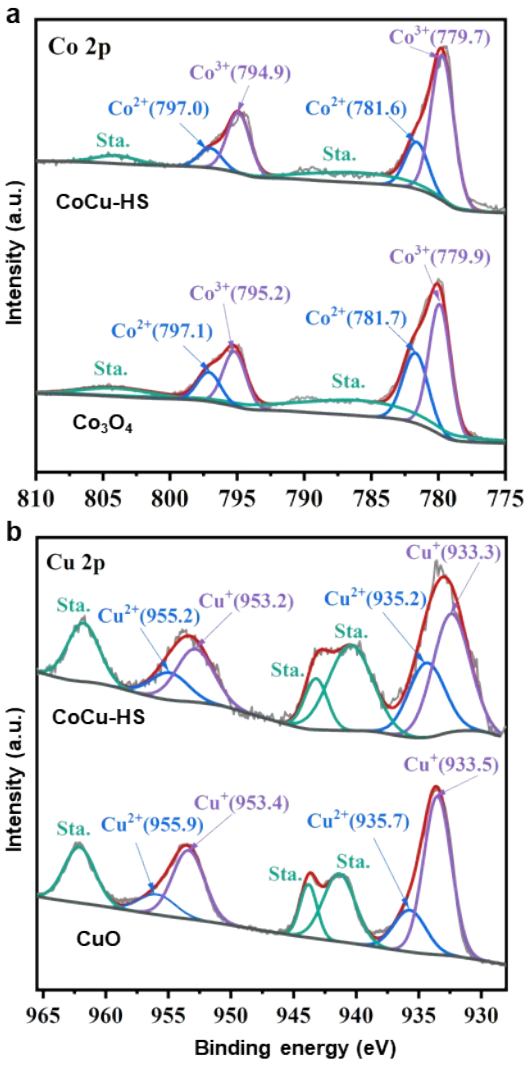

Fig. S12 XPS of (a) Co 2p spectrum and (b) Cu 2p spectrum.

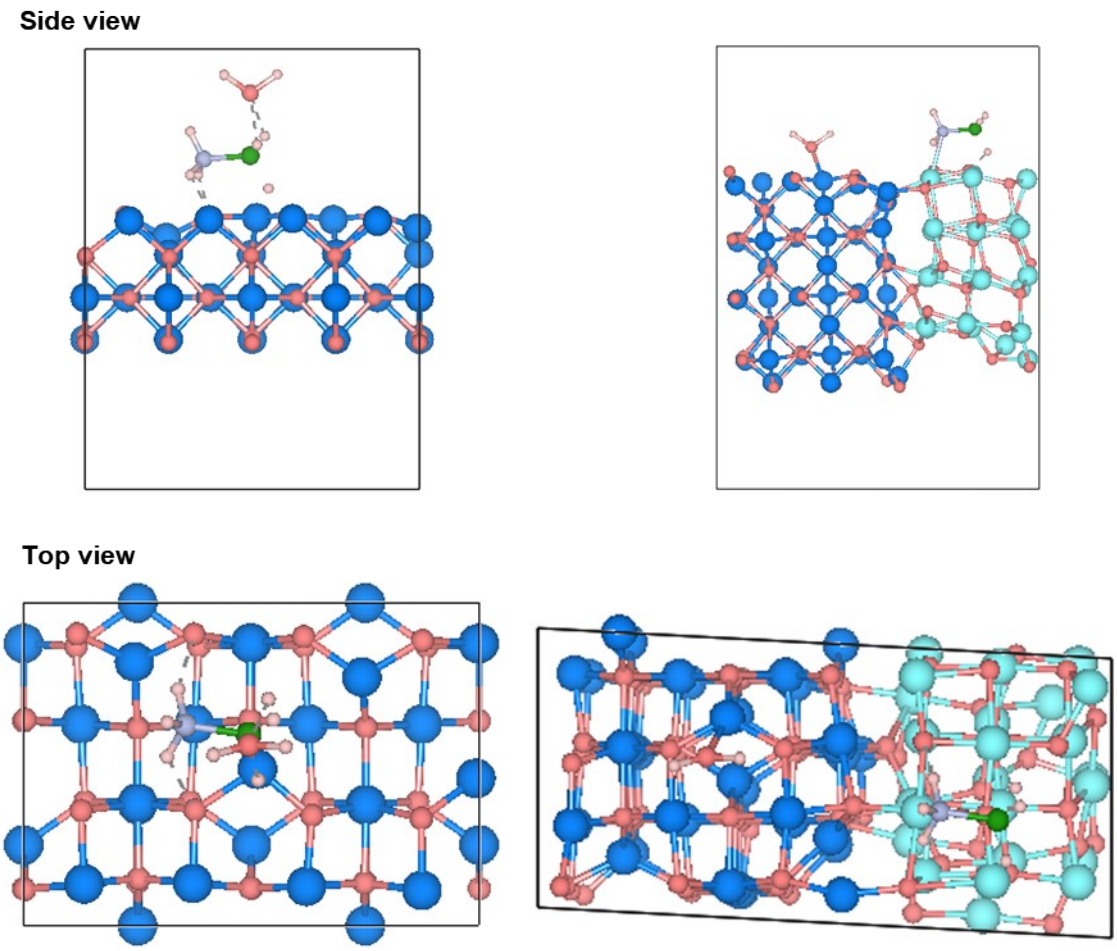

Fig. S13 Top view and side view of H_2O and AB adsorption on Co_3O_4 and CuCo-HS.

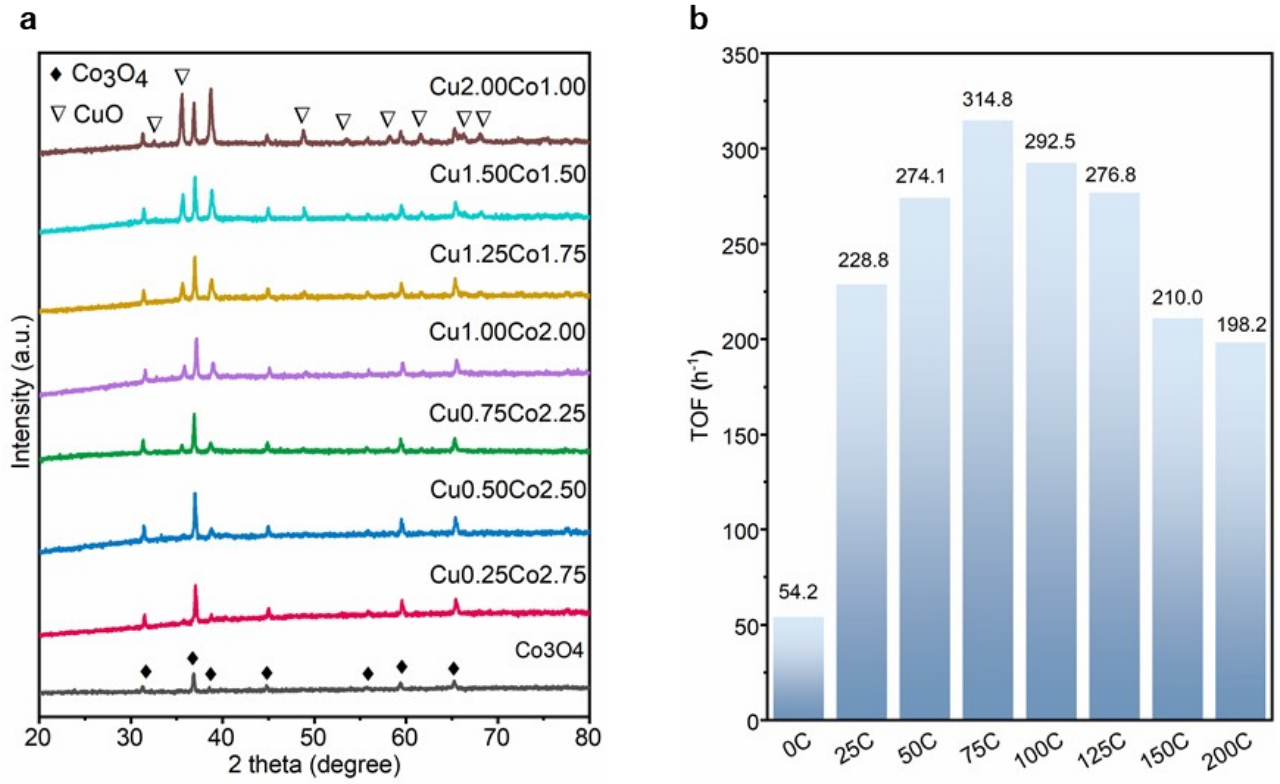

Fig. S14 Influence of different proportions of Cu on Co_3O_4 catalyst: (a) Phase compositions and (b) TOF values.